applied sciences

MDPI

Article

Experimental Analysis of the Current Sensor Fault Detection Mechanism Based on Cri Markers in the PMSM Drive System

Kamila Jankowska and Mateusz Dybkowski *

Department of Electrical Machines, Drives and Measurements, Wroclaw University of Science and Technology, ul. Wybrzeze Wyspianskiego 27, 50-370 Wroclaw, Poland

* Correspondence: mateusz.dybkowski@pwr.edu.pl; Tel.: +48-71-320-3246

Featured Application: The detection system described in the paper can be successfully implemented in industrial drive systems with PMSM motors in order to increase their safety. The natural area of application of FTC (Fault Tolerant Control) systems are electric vehicle drive systems, including electric and hybrid aircraft drive systems.

Abstract: In this paper the current sensor fault detector for the permanent-magnet synchronous motor drive system has been presented. The solution is a known method used for induction motor drive systems, tested by authors in simulation for the PMSM drive system. The application is based on the current markers, which enable not only failure detection, but also the location of said failures. Detector operation is based only on the analysis of measurements from current sensors and does not require additional information about other state variables. The aim of the work is to present simulation and experimental studies in field-oriented control (FOC) for the tested current sensor fault detector for various operating conditions of the drive system—variable speed and load.

Keywords: FTC; PMSM; current sensors; markers

Citation: Jankowska, K.; Dybkowski, M. Experimental Analysis of the Current Sensor Fault Detection Mechanism Based on Cri Markers in the PMSM Drive System. *Appl. Sci.* **2022**, *12*, 9405. https://doi.org/10.3390/app12199405

Academic Editors: Jong-Myon Kim, Cheol Hong Kim and Farzin Piltan

Received: 28 August 2022
Accepted: 16 September 2022
Published: 20 September 2022

1. Introduction

Currently, modern industry uses electric drive systems equipped with advanced diagnostic systems. Such systems are called fault-tolerant control (FTC) [1,2]. FTC systems are divided into two types: passive (PFTC) and active (AFTC) [3]. In passive systems, controllers adjust their parameters to changing operating conditions in the event of a failure; adaptive or neural controllers are used. PFTC somehow compensates for the impact of failure on the control structure. However, this type of a system does not detect failure, so the failure may still progress. They only work well in the early stages of minor failures. Scientists are definitely more interested in active systems. In this case, traditional control structures are equipped with additional blocks for failure detection and compensation. Failure compensation may be hardware- or software-based.

In electric drive systems, failures are divided into three main categories [4]. The first is damage to the electric motor itself. These failures mainly affect the bearings and stator windings. In the event of a bearing failure, the component must be replaced; the failure cannot be compensated [5–8]. Attempts to compensate for stator short circuits were made by using additional redundant windings [9]. This is a typical hardware compensation. Another type of failure mentioned in the literature is the failure of the frequency converter [10–12]. Here, the compensation is usually done by redundant components, e.g., transistors. The detection of both of the above-mentioned failures is performed with the use of measuring sensors, which are the last type of basic failures. Usually, detection is based on current measurement.

PMSM drive systems, which are the subject of research using two or three current sensors, depend on the method of determining the stator current components [13]. Current sensors based on the Hall effect are most often used in drive systems. It is a component that is exposed to many types of damage. Some of them can only worsen the performance of the drive system, and some prevent it completely. This is why fast detection and compensation of their damage are so important. This is essential in sensitive industries such as electric vehicles, the space industry, and the aviation industry. Such sensors provide non-invasive measurements. A conductor with the flowing current is placed in the magnetic core. The Hall sensor is placed in a small air gap. The magnetic field generated by the conductor is recreated on the secondary winding. The magnetic field is then detected by a Hall sensor and a voltage proportional to the conductor current is generated at its output [14]. Damage in such a sensor may be caused by the corrosion of the core, changes in the magnetic properties of the ferrite core due to temperature, or, e.g., changes in the orientation of the magnetic field induced in the sensor [15]. These damages can lead to a complete break of the sensor and loss of measurement signal or phase shift, noise, and gain changes.

Current sensor fault detection methods are divided into signal-based [16,17] and model-based [18,19]. State variable observers are used in model-based methods, which require the knowledge of motor parameters [20]. Most of them depend heavily on them. Correct operation requires precise parameterization. Different parameters are used depending on the observer type, but the stator resistance and inductance are reproducible for most of them. However, these are parameters whose values change over time. This may worsen the estimation properties. A significant advantage of this type of method is that the estimator used for detection can also be used to compensate for failures.

In the paper [21], the authors described a sliding-mode observer (SMO) for the detection of faults in current sensors in the PMSM control system. Online diagnostics of the ABC phase current sensor failure is performed based on the relationship between residual errors, generated by SMO and phase current sensor errors and the rules of failure diagnostics. The paper presents experimental and simulation results, but only for two types of faults: gain and offset fault. These are failures that do not significantly affect the entire control structure.

Paper [22] describes the use of a different type of observer—the extended Kalman filter (EKF). Detection is performed by comparing the estimated values with the measured ones. The work presents experimental results for one type of current sensor fault—a signal loss for one speed value.

The detection of current and speed sensors is described in the article [23]. Two types of observers are used for this purpose: high-order sliding mode (HOSM) and Luenberger observer (LO). LO is responsible for current estimation. The measurement of speed and α, β voltages were used for estimation. These values are compared with the measured values of stator currents; if the difference between them exceeds a certain fixed value, it means a failure in the corresponding phase. In the work under experimental conditions, the detection of signal loss in phase A was shown.

Signal-based methods do not require knowledge of the object model [24]. Once implemented, the algorithm is a universal solution for motors with different parameters. These algorithms are also usually of low computational complexity and can be easily implemented in a signal processor. These are their most important advantages.

An example of a signal-based method can be seen in the research presented in [25]. The detection and localization of the current sensors are based on current measurements. The authors described a simple detector that compares average normalized values of the phase currents in three phases. The phase shift between the remaining phases after the failure occurred is also taken into account. Only the detection of the measurement signal loss is considered in the research. This method is also described in [26].

Another simple solution is shown in the article [27]. The authors used the fact that in the event of a failure of one of the current sensors, the phase shift between the other two changes and the sign of current value (SCV) is also used for detection.

A method based on signal measurements is also described in the article [28]. Current sensor fault detection is based on the measurement of the voltage in the intermediate circuit. There are also examples in the literature where detection is based on the measurement of other quantities, such as current [25] or rotor position. There are also works in which the measurement of several signals is used to detect faults in current sensors [29].

This article describes a method based on measurement signals. It uses only the current measurement to detect faults in the current sensors. The method consists of determining the so-called current markers and then comparing their values. The method was previously described for induction motors [24]. Simulation tests for the PMSM in field-oriented control and experimental results in scalar control are also presented [30]. The fault diagnostic system was tested in simulation in two control algorithms—the scalar control and vector control—to demonstrate the transient of faulted signals, detection signals, and detection time. In this position, it is shown that after current sensor fault appearance, its influence on the control structure, especially speed transient, is compensated using non-sensitive components. The analysis is presented for all the above-mentioned faults for different speed conditions.

This study describes its application in experimental research in the control structure field-oriented control (FOC). In FOC, when one of the sensors fails, it affects the entire control structure. After fault high currents appear, the rated values are exceeded several times. This definitely makes it difficult to locate the failure. Each sensor shows an abnormal value. That is why it is so important to conduct experimental research in a closed-loop structure. Adequately short detection time in the presented method allows us to locate a damaged sensor before incorrect measurement has a significant effect on the entire control structure. For most failures, it is detected in the second sample after it occurs. Apart from failure detection, the proposed solution also allows for its compensation. Hardware compensation was used here. The third current sensor, in phase C, is used to determine the stator components in the event of a sensor failure in phase A or B. The paper presents the detection of:

- signal loss;
- signal interruption;
- variable gain;
- measurement noise.

The literature usually describes the detection of one failure—signal loss. Additionally, in the above-mentioned works, no tests were carried out for different speed or load values. The results of detection in the dynamic states of the system operation are not presented either. The proposed solution is universal both for failures with a large impact on the control structure and those with a small one.

The article is organized as follows: The first chapter provides an overview of methods for detecting faults in current sensors in drive systems. The next chapter describes the control structure, which was used in both simulation and experimental studies. The third chapter presents the theoretical basis of the fault detection algorithm and the method of their compensation. The fourth and fifth parts of the article show the simulation and experimental results, respectively. The last chapter contains a brief summary of the results and further research plans.

2. Control Structure of PMSM Drive System with a Detection Mechanism

In the presented research, the field-oriented control structure was used. This structure was supplemented with blocks for simulation, detection, and compensation of the failure of current sensors. The damages were simulated in a software manner. The equations used to simulate individual failures are presented in Table 1.

Table 1. Equations to simulate individual failures of current sensors.

Type of the Fault	Current Value
Variable gain	$i_s^m = (1-\gamma)i_a$
Signal limit	$i_s^m = i_{sat}$
Noise	$i_s^m = i_a + n(t)$
Lack of signal	$i_s^m = 0$
Intermittent signal	$i_s^m = [0, 1]$

where i_s^m—fault current, i_a—measured current, γ—constant value from the range <−1, 1>.

In the article, both for simulation and experimental tests, a surface-mounted 0.894 kW PMSM with the parameters presented in Table 2 was used.

Table 2. Parameters of the motor used in simulation and experimental results.

P_N [kW]	P_p [-]	Ω_N [rpm]	T_N [Nm]	I_N [A]	J [kg·m^2]	R_s [Ω]
0.894	4	6200	1.4	1.9	0.000039	4.6615

P_N—nominal power, Pp—pool pairs, Ω_N—nominal speed, T_N—nominal torque, I_N—nominal stator current, J—inertia, Rs—stator phase resistance.

The structure of the field-oriented control ensures very good operating parameters of the drive system, because of the use of current sensors. In the conducted tests, two current sensors are used for control, in phases A and B. The sensor in phase C is used only for failure detection and compensation. A two-level inverter with a 10 kHz switching frequency was used in the research. The scheme of the control structure is shown in Figure 1.

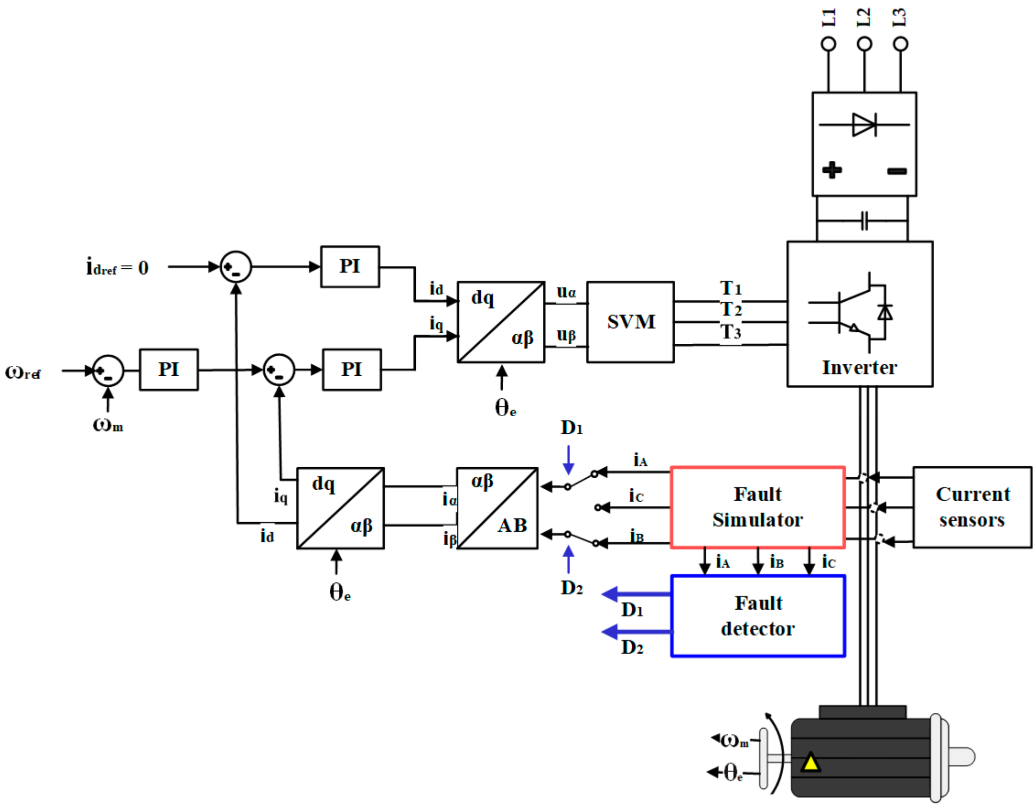

Figure 1. Block diagram of the control structure.

3. Detection Mechanism Based on Cri Markers

For the correct operation, the drive system with PMSM requires at least two current sensors. In the analyzed example, the third sensor is used only for diagnostics. The basis of the detection algorithm is the fact that the i_α and i_β current components used in the control structure can be determined using different equations depending on the phases in which the measurement is performed [24]:

$$i_{\alpha 1} = \frac{2}{3}(i_A - \frac{1}{2}(i_B + i_C)), i_{\beta 1} = \frac{\sqrt{3}}{3}(i_B - i_C), \tag{1}$$

$$i_{\alpha 3} = -(i_B + i_C), i_{\beta 3} = -\frac{\sqrt{3}}{3}(i_B - i_C), \tag{2}$$

$$i_{\alpha 2} = i_A, i_{\beta 2} = \frac{\sqrt{3}}{3}(i_A + 2i_B) \tag{3}$$

On the basis of these equations, it is possible to determine current markers that are insensitive to the measurement of one of the phases:

$$C_{ri1} = (i^2_{\alpha 3} + i^2_{\beta 1}), C_{ri2} = (i^2_{\alpha 2} + i^2_{\beta 3}), C_{ri3} = (i^2_{\alpha 2} + i^2_{\beta 2}), \tag{4}$$

After transformations, the following formulae are obtained:

$$C_{ri1} = (-(i_B + i_C))^2 + (\frac{\sqrt{3}}{3}(i_B - i_C))^2, \tag{5}$$

$$C_{ri2} = (i_A)^2 + (-\frac{\sqrt{3}}{3}(i_A + 2i_C))^2, \tag{6}$$

$$C_{ri3} = (i_A)^2 + (\frac{\sqrt{3}}{3}(i_A + 2i_B))^2. \tag{7}$$

However, based on the values of the markers themselves, the location of the damaged phase would not always be clear and stable. Therefore, the algorithm uses the difference in the value of markers from the current and previous samples—the so-called marker errors. This ensures stable detection:

$$\Delta C_{rij} = \left|C_{rij}(k) - C_{rij}(k-1)\right|. \tag{8}$$

The last element of the algorithm is an additional condition—*Delta* relating to the i_α and i_β values determined with the use of various current sensors:

$$(i_{\alpha 1} = i_{\alpha 2} = i_{\alpha 3}) \wedge (i_{\beta 1} = i_{\beta 2} = i_{\beta 3}). \tag{9}$$

The relations between the marker error values depending on the damaged phase are repeatable. On this basis, the detector not only detects damage to the current sensor, but also locates the damaged phase. Table 3 summarizes the relationship between marker errors, which are confirmed by the following simulation and experimental results.

Table 3. Dependencies between marker errors during failure in particular phases.

Type of Fault	ΔCrij
No fault	ΔCri1 = ΔCri2 = ΔCri3
Phase A sensor	ΔCri2 < ΔCri3 < ΔCri1
Phase B sensor	ΔCri1 < ΔCri3 < ΔCri2

Figures 2–4 show the marker error transients and detector responses at the time of different failures in phases A and B in simulation and experimental tests. The detector has two outputs. The first output, D1, refers to phase A, and the second, D2, refers to phase B. Value 0 at the detector output means no failure, and 1 at the output means failure in the corresponding phase.

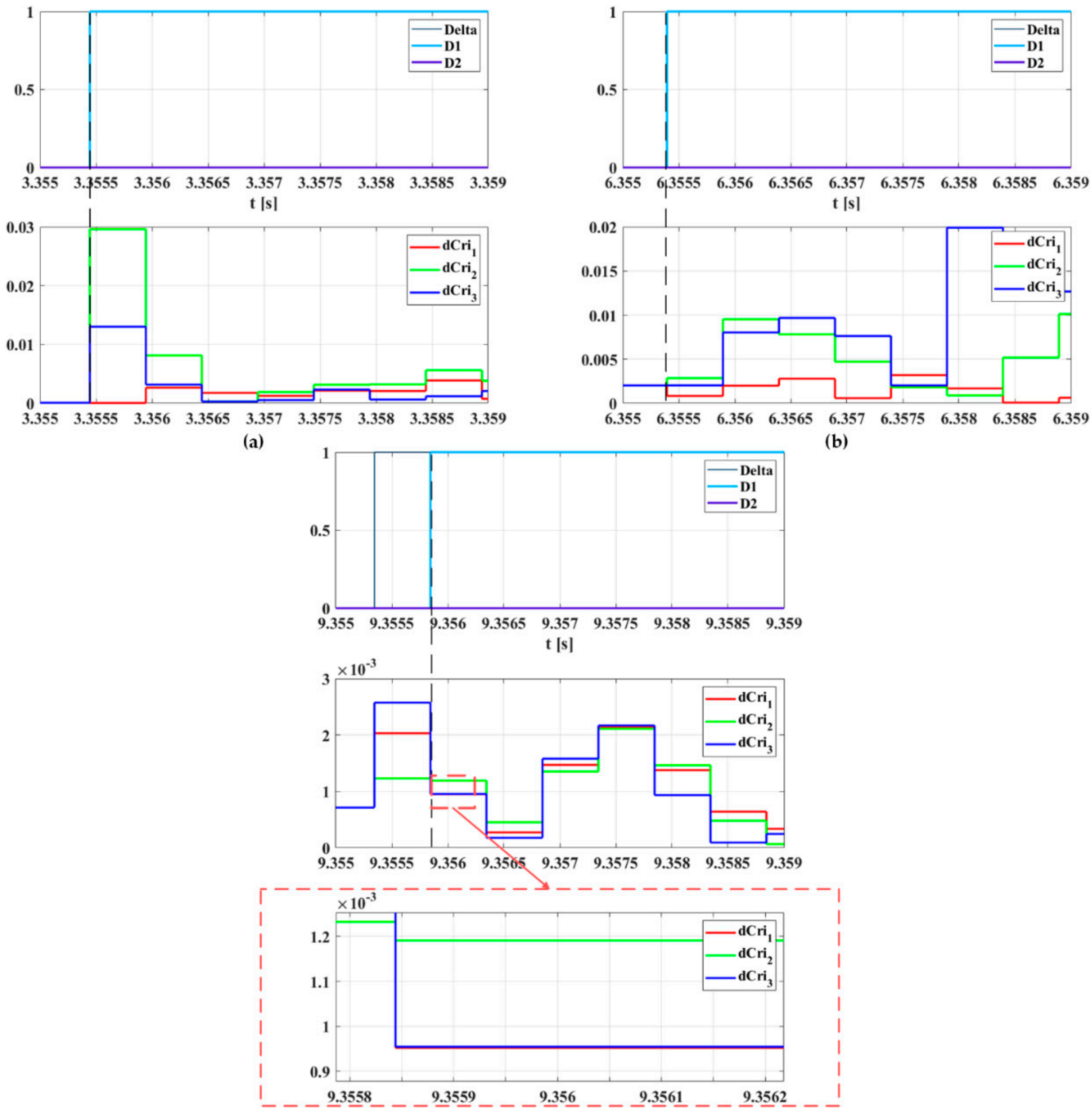

(c)

Figure 2. Detector responses and transients of marker errors during lack of signal: (**a**) measurement white Gaussian noise (70 dB); (**b**) variable gain; (**c**) (1.2 i_a); in phase A in experimental tests.

On the basis of Figures 2 and 3, it is possible to determine the relationships that appear between the marker errors in phase A after the failure. The simulation and experimental results are consistent. Furthermore, in both simulation and experimental tests, not every type of failure was detected in the sample after its occurrence. The detection of failures that have a smaller impact on the control structure, such as measurement noise or variable gain, takes longer.

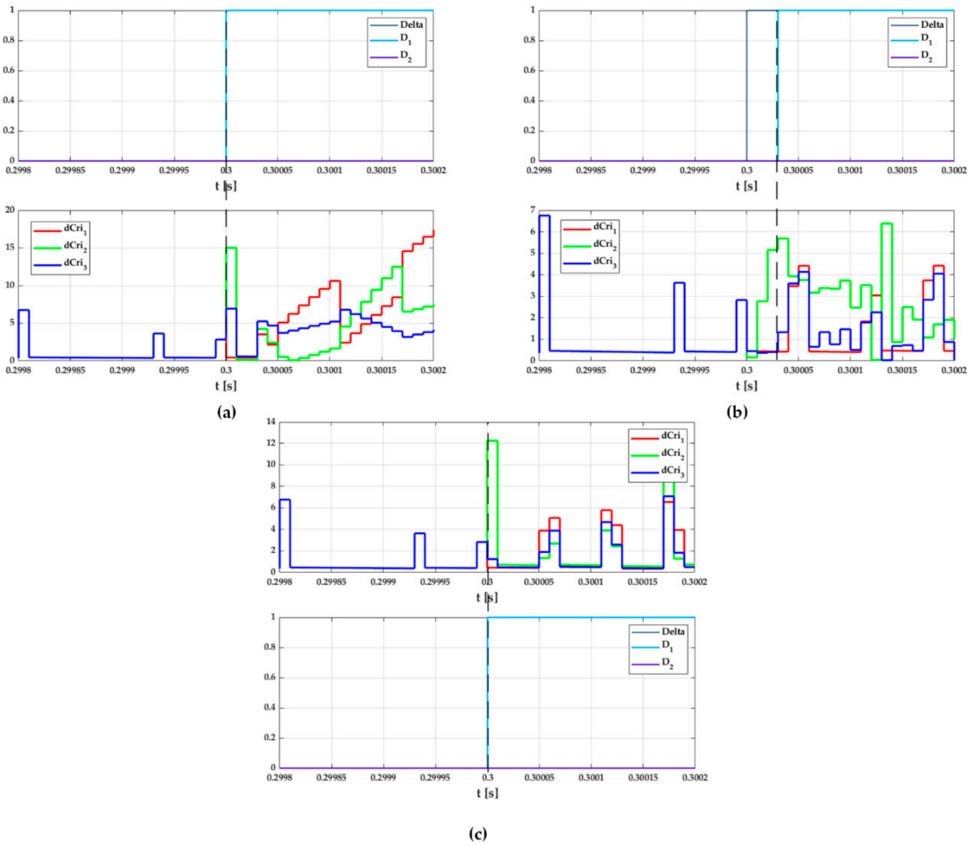

Figure 3. Detector responses and transients of marker errors during lack of signal: (**a**) measurement white Gaussian noise (20 dB); (**b**) variable gain (1.2 i_a); (**c**) in phase A in simulation tests.

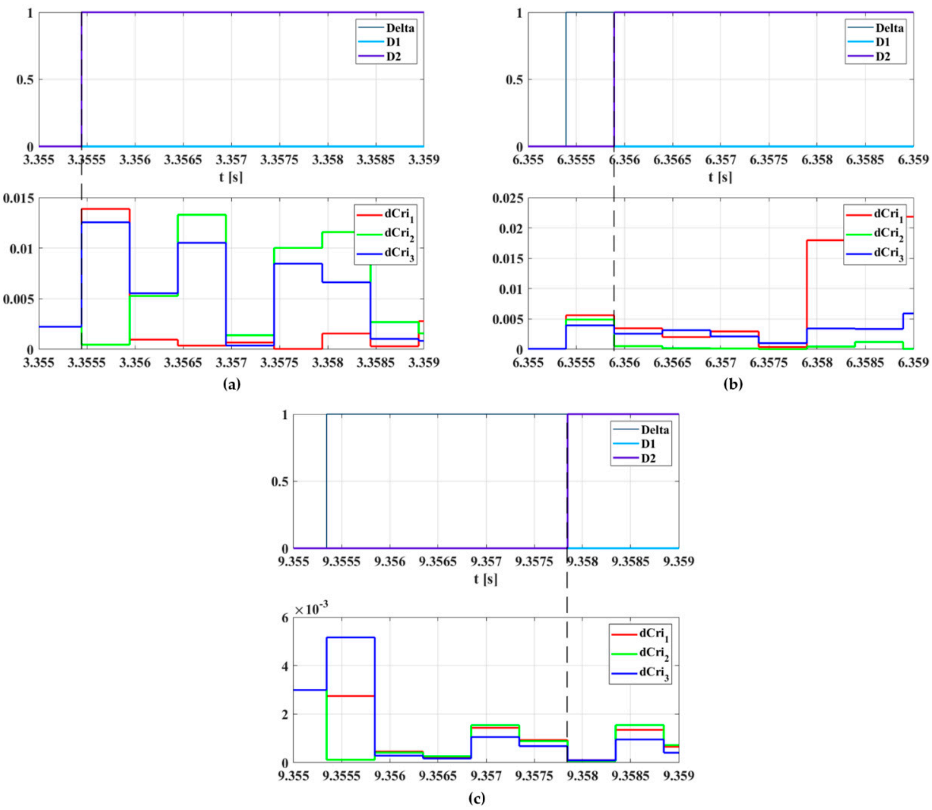

Figure 4. Detector responses and transients of marker errors during lack of signal: (**a**) measurement white Gaussian noise (70 dB); (**b**) variable gain (1.2 i_a); (**c**) in phase B in experimental tests.

Figures 3 and 4 show respective results for the failures in phase B. In this case, the simulation tests are also consistent with the experimental ones.

Figures 2–5 show that during normal drive operation, when the sensors are not damaged, the dCri$_{1\text{-}3}$ signals coincide with each other. This is due to the principle of the detector operation. When all types of damage occur, the signals differ from each other. This signal is based on signals from undamaged sensors for a smaller increment; the other two use the signal from the damaged sensor. In this way, the fault can be easily detected. Importantly, the detection time is counted in individual samples which, on the one hand, is an advantage of the system. On the other hand, if no failure is detected in the first three samples, subsequent samples will not detect it.

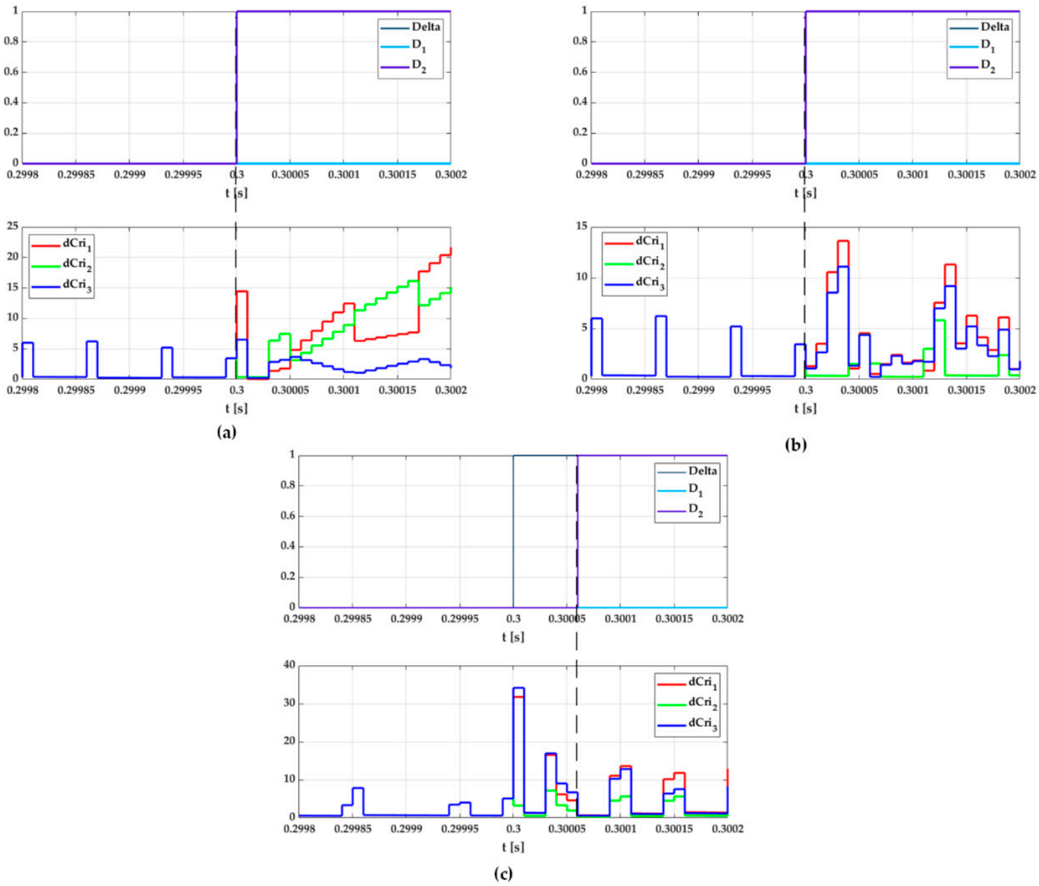

Figure 5. Detector responses and transients of marker errors during lack of signal: (**a**) measurement white Gaussian noise (20 dB); (**b**) variable gain (1.2 i_a); (**c**) in phase B in simulation tests.

4. Simulation Results

The simulation tests were carried out in the Matlab/Simulink environment. The model of the control structure was made in Sim Power System toolbox. The Euler method was used with fixed step size equal to 1×10^{-5} s.

Figure 6 shows the detector responses obtained with a periodic signal interruption for different speed reference values. When the signal is interrupted, the stator current reaches several times the rated value. A greater impact on the operation of the drive system can be observed during failure in phase B. There are disturbances in the speed at the moments of signal interruption. It can also be seen in the transients of speed errors. In the event of a failure in phase B, the deviations from the set point are greater. The detector correctly recognizes the damaged phase at low, medium, and high speeds in both dynamic and steady states.

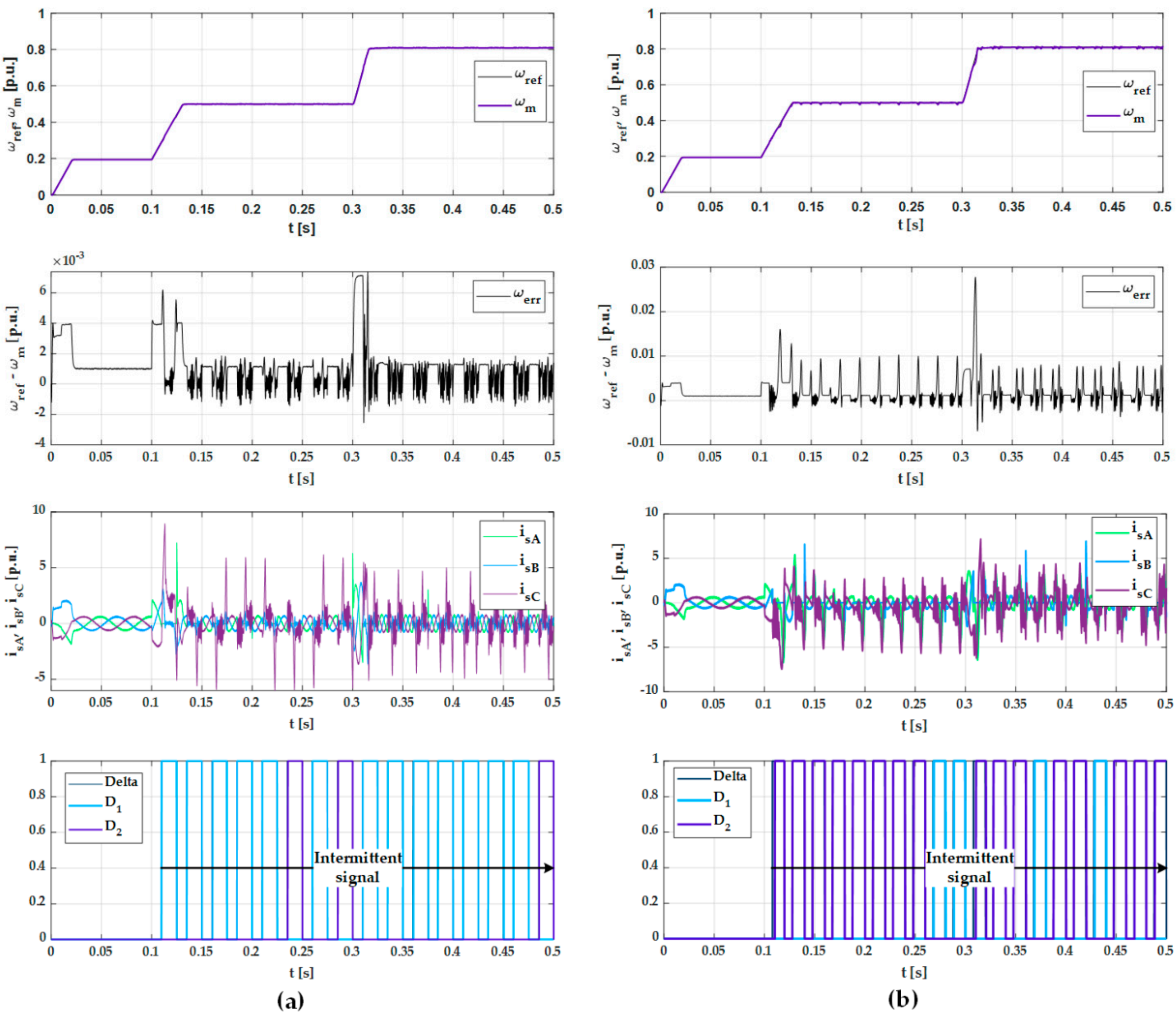

Figure 6. Detector responses obtained with a periodic signal interruption for different speed reference values for phase A (**a**) and phase B (**b**).

Figure 7 shows the detection of less significant types of failures. The results are shown for variable gain in phase A (1.2 i_a) and white Gaussian noise (20 dB) in phase B. The impact of this type of failure is imperceptible in speed, as seen in the speed error transients. Despite the insignificant impact on the control structure, the failure is correctly detected and located. Additionally, the detector correctly recognizes a failure, even in dynamic states.

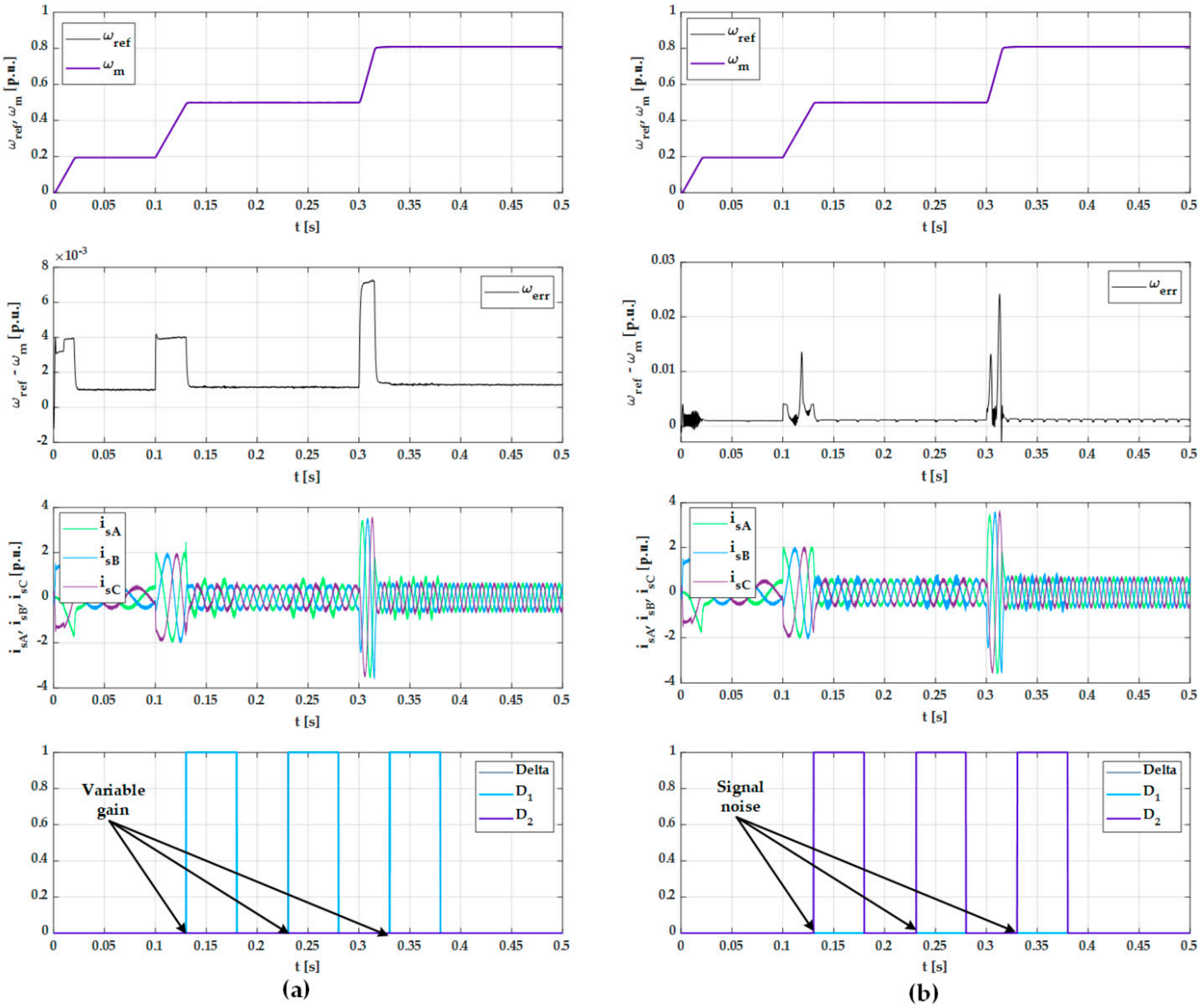

Figure 7. Detector responses and state variable transients during variable gain (1.2 i_a); in phase A (**a**) and measurement noise (20 dB) in phase B (**b**).

5. Experimental Results

The experimental test was conducted on a 0.894 kW surface-mounted PMSM (Table 2) by Moog (G403-2007A). A dSpace DS1103 with Control Desk was used as a controller in the tests; the position was measured with an incremental encoder (36000 imp./rot), while the current measurement was performed with current LEM transducers. Another Moog servo drive-controlled motor was used as a load (G404-2009A). Photos of the laboratory set-up are presented in Figure 8. A frequency converter with the ability to control transistors was used. The switching frequency was 10 kHz. The tests were performed in the DFOC system. Classical PI controllers with an anti-windup system were used. The experimental tests were carried out for the low range of speed values (0–0.3ω_N) and two load values (0.1 T_N and 0.2 T_N). The detector responses to the lack of signal, signal interruption, measurement noise (70 dB white Gaussian noise), and variable gain were checked. The damages were simulated in a software manner. All results are presented as per unit.

Figures 9 and 10 show the detection of variable gain with γ value equal to 0.2 in phase A and measurement noise in phase B with a parameter of 70 dB for two velocity values. The detector correctly detects and locates the failure in dynamic and stable states. Those failures do not significantly affect the control structure and the differences between marker errors are small.

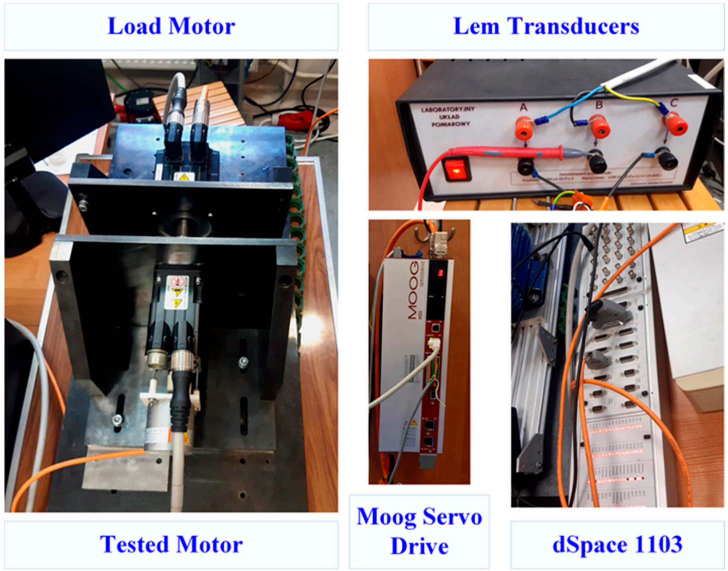

Figure 8. Photos of experimental set-up elements.

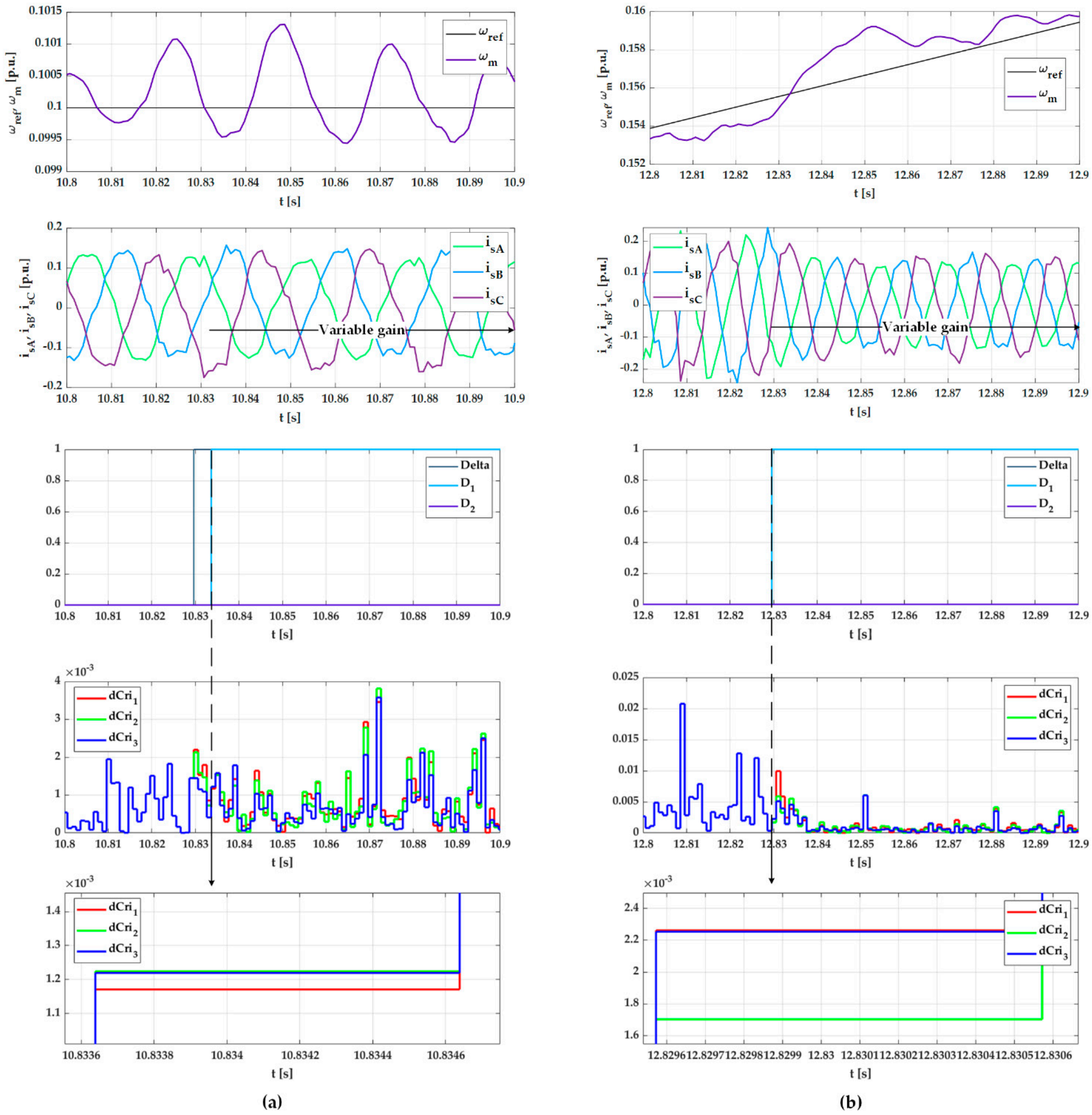

Figure 9. Transients of speed, stator currents, detector responses, and marker errors during variable gain (γ = 0.2) in phase A for different speed values in stable (**a**) and dynamic (**b**) states.

Figure 10. Transients of speed, stator currents, detector responses, and marker errors during signal noise (70 dB) in phase B for different speed values in stable (**a**) and dynamic (**b**) states.

The effectiveness of the detector during intermittent signals in phase A and B with the motor load for different values is shown in Figure 11. This type of failure interferes with the speed transient. It is especially visible for the lowest values. The figure also shows the difference between the reference speed and the measured speed. At the time of failure, the difference increases noticeably.

A detailed analysis of the effect of signal interruption is shown in Figure 11. The occurrence of a failure causes a significant increase in the oscillation of the speed and the value of the stator current. This is because the stator current components i_α and i_β are not correctly determined, as also shown in the figure.

As the detector based on Cri markers locates the failure, it also allows for its compensation.

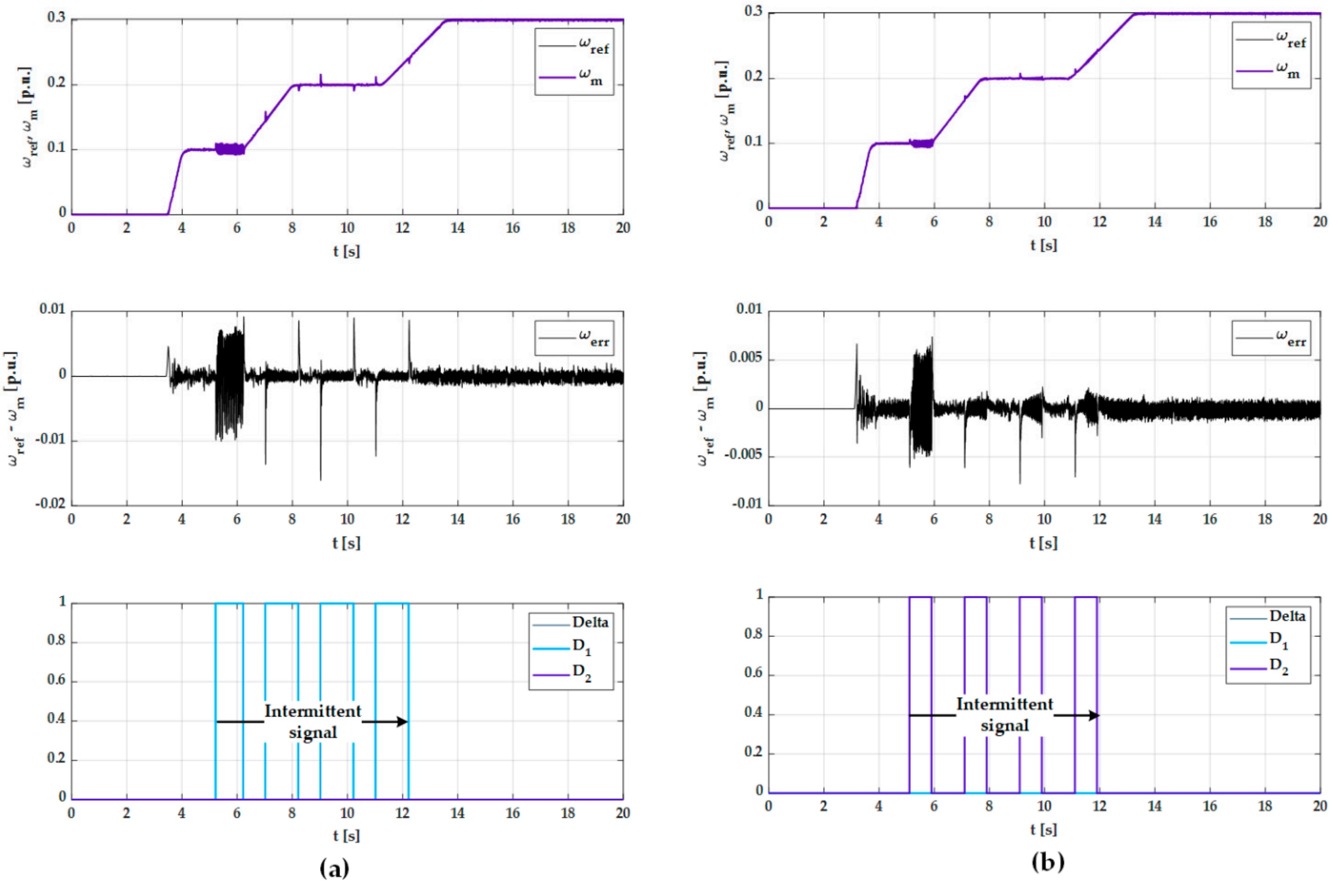

Figure 11. Transients of speed, speed error and detector response during signal interruptions in phase A with a motor load of 0.1 T_N (**a**) and phase B with a load of 0.2 T_N (**b**).

Figure 12 shows failure compensation using phase C's redundant sensor. Despite the loss of the signal in one of the phases, the stator current components i_α and i_β are determined correctly, and the current transients in the remaining phases are undisturbed. There are no transient distortions as in Figure 12, where the system is shown without damage compensation.

The transients showing the effectiveness of detection and compensation under the condition of periodic signal interruption are shown in Figures 13 and 14 in phase A and phase B, respectively. Signal interruptions occur with a high frequency. The system adapts dynamically to work in failure states and in the absence of damage to the current sensors. Disturbances in the operation of the system do not appear even in dynamic states. The only disturbance in speed can be observed when, during the failure in phase B, the detector did not correctly recognize the damaged phase; as a result, the compensation mechanism did not work (Figure 15). Based on the speed error transient, it can also be seen that a significant deviation appears when the compensation mechanism does not work.

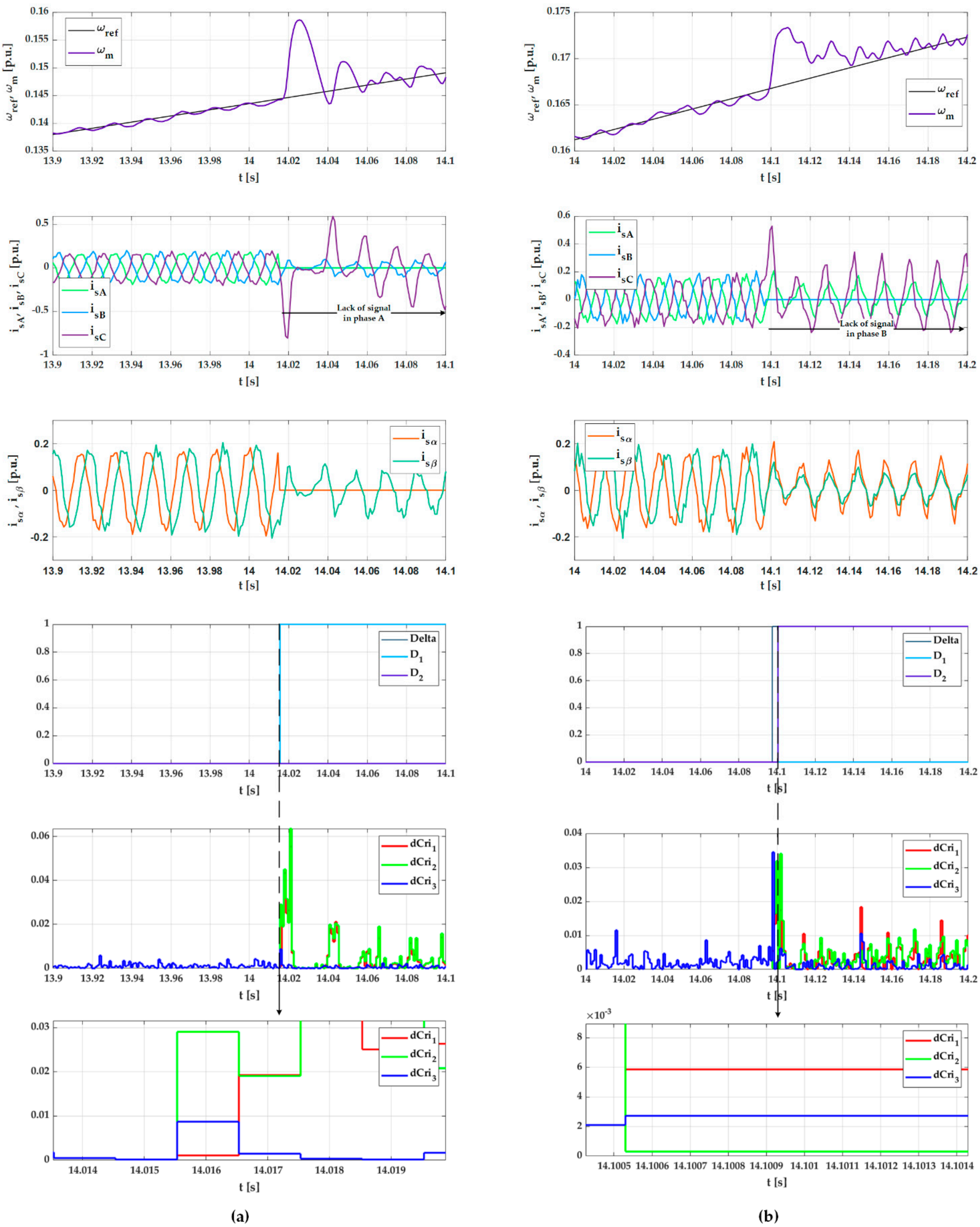

Figure 12. Transients of speed, stator currents, stator current components, detector response, and marker errors during signal interruptions without motor load in phase A (**a**) and B (**b**).

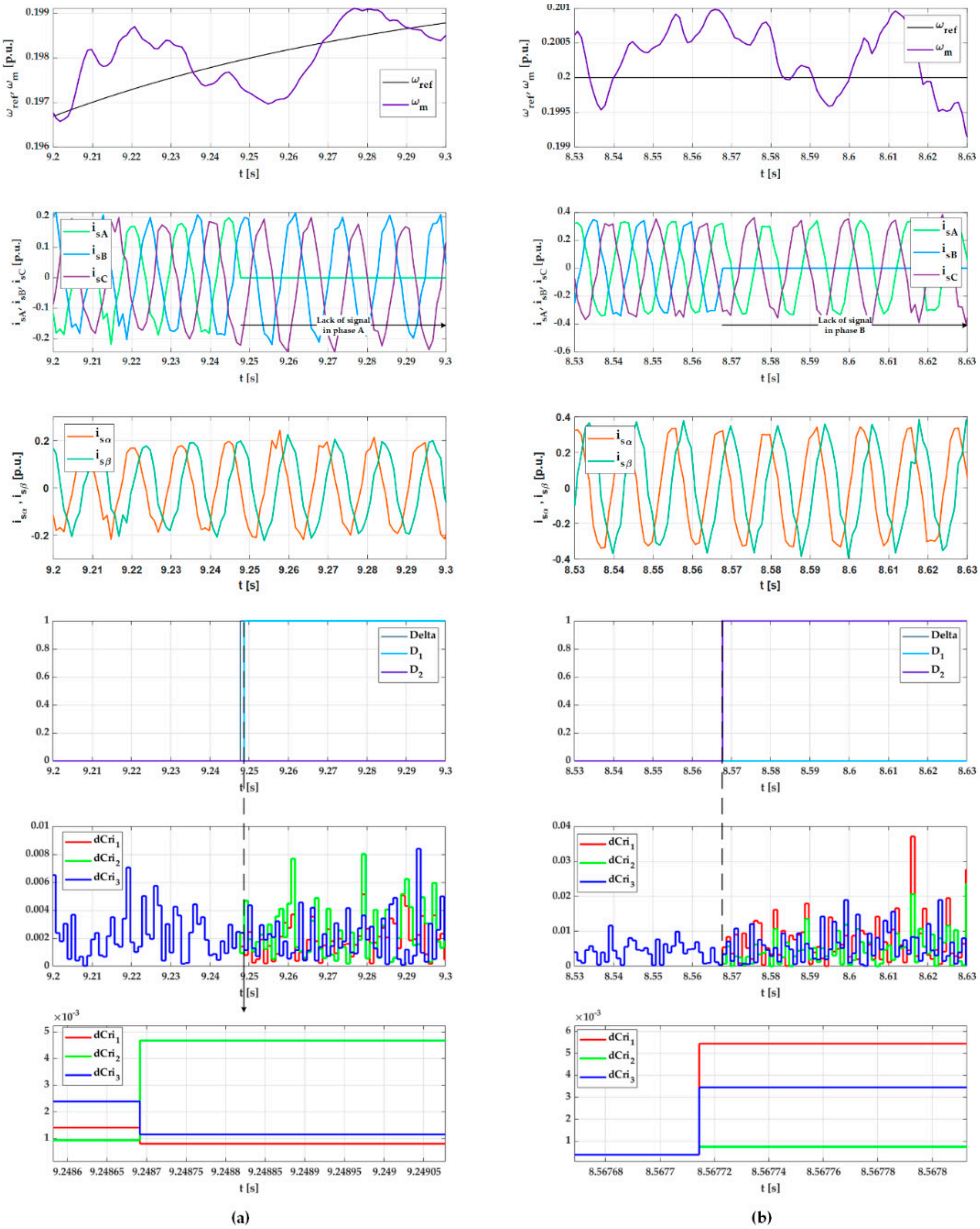

Figure 13. Transients of stator currents, stator current components—i_α, i_β, detector response, and marker error transients during lack of signal in phase A (**a**) and B (**b**) in control structure with compensation mechanism.

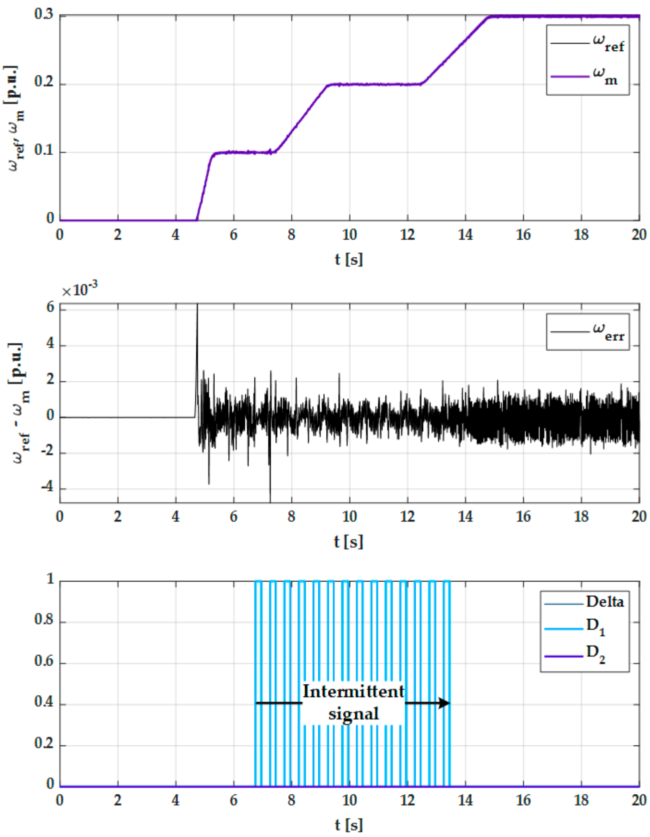

Figure 14. Transients of speed, speed error, and detector response during dynamic interruptions in phase A in a structure with damage compensation.

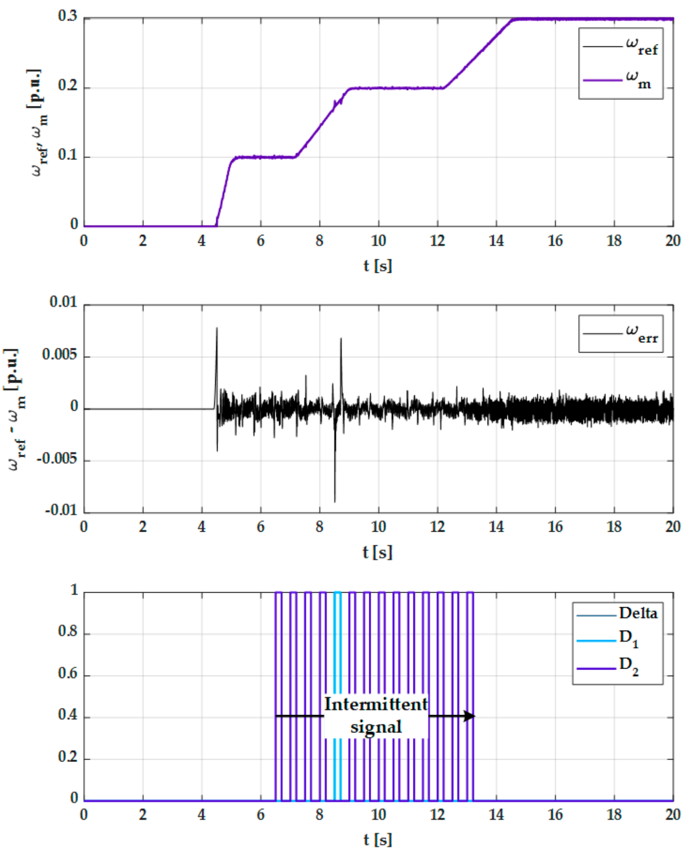

Figure 15. Transients of speed, speed error, and detector response during dynamic interruptions in phase B in a structure with damage compensation.

6. Conclusions

The article presents the algorithm for fault detection of current sensors in the PMSM control system. The proposed solution is a method based on measurement signals. It is based on the dependencies between current markers. The work presents simulation and experimental tests that are consistent with each other and confirm the effectiveness of the detection algorithm for different values of speed and motor load. The detector operation is also correct with the unloaded motor. The most important advantages of the application that should be emphasized are:

- Short detection time, usually in the first or second sample after the failure has occurred;
- Detection of many types of failures, even those with an insignificant impact on the control structure;
- Correct detection in dynamic states for different speed and load values;
- No requirement to know the motor parameters, which makes the proposed solution universal for PMSM systems of different-rated power;
- Possibility to use in FTC system.

In further research, it is planned to use the algorithm in the direct torque control structure.

Author Contributions: Conceptualization, M.D., K.J.; methodology, M.D., K.J.; software, K.J.; validation, M.D., K.J.; formal analysis, M.D., K.J.; investigation, K.J.; resources, M.D., K.J.; data curation, K.J.; writing—original draft preparation, K.J.; writing—review and editing, M.D.; visualization, K.J.; supervision, M.D.; project administration, M.D.; funding acquisition, M.D. All authors have read and agreed to the published version of the manuscript.

Funding: This research received no external funding.

Institutional Review Board Statement: Not applicable.

Informed Consent Statement: Not applicable.

Data Availability Statement: Not applicable.

Acknowledgments: This research was supported by statutory funds of the Faculty of Electrical Engineering, Wroclaw University of Science and Technology (2022).

Conflicts of Interest: The authors declare no conflict of interest.

References

1. Klimkowski, K.; Dybkowski, M. A Fault Tolerant Control Structure for an Induction Motor Drive System. *Automatika* **2016**, *57*, 638–647. [CrossRef]
2. Wang, G.; Hao, X.; Zhao, N.; Zhang, G.; Xu, D. Current Sensor Fault-Tolerant Control Strategy for Encoderless PMSM Drives Based on Single Sliding Mode Observer. *IEEE Trans. Transp. Electrif.* **2020**, *6*, 679–689. [CrossRef]
3. Guezmil, A.; Berriri, H.; Pusca, R.; Sakly, A.; Romary, R.; Mimouni, M.F. Experimental Investigation of Passive Fault Tolerant Control for Induction Machine Using Sliding Mode Approach. *Asian J. Control* **2019**, *21*, 520–532. [CrossRef]
4. Wu, C.; Guo, C.; Xie, Z.; Ni, F.; Liu, H. A Signal-Based Fault Detection and Tolerance Control Method of Current Sensor for PMSM Drive. *IEEE Trans. Ind. Electron.* **2018**, *65*, 9646–9657. [CrossRef]
5. Wang, X.; Lu, S.; Huang, W.; Wang, Q.; Zhang, S.; Xia, M. Efficient Data Reduction at the Edge of Industrial Internet of Things for PMSM Bearing Fault Diagnosis. *IEEE Trans. Instrum. Meas.* **2021**, *70*, 3508612. [CrossRef]
6. Wagner, T.; Sommer, S. Bearing fault detection using deep neural network and weighted ensemble learning for multiple motor phase current sources. In Proceedings of the 2020 International Conference on Innovations in Intelligent SysTems and Applications (INISTA), Novi Sad, Serbia, 24–26 August 2020; pp. 1–7. [CrossRef]
7. Siddiqui, K.M.; Bakhsh, F.I.; Ahmad, R.; Solanki, V. Advanced Signal Processing Based Condition Monitoring of PMSM for Stator-inter Turn Fault. In Proceedings of the 2021 IEEE 8th Uttar Pradesh Section International Conference on Electrical, Electronics and Computer Engineering (UPCON), Dehradun, India, 11–13 November 2021; pp. 1–4. [CrossRef]
8. Skowron, M.; Orlowska-Kowalska, T.; Kowalski, C.T. Application of simplified convolutional neural networks for initial stator winding fault detection of the PMSM drive using different raw signal data. *IET Electr. Power Appl.* **2021**, *15*, 932–946. [CrossRef]
9. Canseven, H.T.; Ünsal, A. Performance Improvement of Fault-Tolerant Control for Dual Three-Phase PMSM Drives Under Inter-Turn Short Circuit Faults. In Proceedings of the IECON 2021—47th Annual Conference of the IEEE Industrial Electronics Society, Toronto, ON, Canada, 13–16 October 2021; pp. 1–5. [CrossRef]
10. Kontarček, A.; Bajec, P.; Nemec, M.; Ambrožič, V.; Nedeljković, D. Cost-Effective Three-Phase PMSM Drive Tolerant to Open-Phase Fault. *IEEE Trans. Ind. Electron.* **2015**, *62*, 6708–6718. [CrossRef]

11. Yan, H.; Xu, Y.; Cai, F.; Zhang, H.; Zhao, W.; Gerada, C. PWM-VSI Fault Diagnosis for a PMSM Drive Based on the Fuzzy Logic Approach. *IEEE Trans. Power Electron.* **2019**, *34*, 759–768. [CrossRef]
12. El Khil, S.K.; Jlassi, I.; Cardoso, A.J.M.; Estima, J.O.; Mrabet-Bellaaj, N. Diagnosis of Open-Switch and Current Sensor Faults in PMSM Drives Through Stator Current Analysis. *IEEE Trans. Ind. Appl.* **2019**, *55*, 5925–5937. [CrossRef]
13. Zhang, G.; Wang, G.; Wang, G.; Huo, J.; Zhu, L.; Xu, D. Fault Diagnosis Method of Current Sensor for Permanent Magnet Synchronous Motor Drives. In Proceedings of the 2018 International Power Electronics Conference (IPEC-Niigata 2018—ECCE Asia), Niigata, Japan, 20–24 May 2018; pp. 1206–1211. [CrossRef]
14. Rudnicki, T. Measurement of the PMSM Current with a Current Transducer with DSP and FPGA. *Energies* **2020**, *13*, 209. [CrossRef]
15. Mehta, H.; Thakar, U.; Joshi, V.; Rathod, K.; Kurulkar, P. Hall sensor fault detection and fault tolerant control of PMSM drive system. In Proceedings of the 2015 International Conference on Industrial Instrumentation and Control (ICIC), Pune, India, 28–30 May 2015; pp. 624–629. [CrossRef]
16. Klimkowski, K.; Dybkowski, M. Adaptive fault tolerant direct torque control structure of the induction motor drive. In Proceedings of the International Conference on Electrical Drives and Power Electronics (EDPE), Tatranska Lomnica, Slovakia, 21–23 September 2015; pp. 7–12.
17. Beddek, K.; Merabet, A.; Kesraoui, M.; Tanvir, A.A.; Beguenane, R. Signal-Based Sensor Fault Detection and Isolation for PMSG in Wind Energy Conversion Systems. *IEEE Trans. Instrum. Meas.* **2017**, *66*, 2403–2412. [CrossRef]
18. Isermann, R. *Fault-Diagnosis Applications, Model-Based Condition Monitoring: Actuators, Drives, Machinery, Plants, Sensors, and Fault-Tolerant Systems*; Springer: Berlin, Germany, 2011.
19. Adouni, A.; Hamed, M.B.; Flah, A.; Sbita, L. Sensor and actuator fault detection and isolation based on artificial neural networks and fuzzy logic applicated on Induction motor. In Proceedings of the International Conference on Control, Decision and Information Technologies (CoDIT), Hammamet, Tunisia, 6–8 May 2013.
20. Bahri, I.; Naouar, M.; Slama-Belkhodja, I.; Monmasson, E. FPGA-Based FDI of Faulty Current Sensor in Current Controlled PWM Converters. In Proceedings of the EUROCON 2007—The International Conference on "Computer as a Tool", Warsaw, Poland, 9–12 September 2007; pp. 1679–1686.
21. Huang, G.; Fukushima, E.F.; She, J.; Zhang, C. Current Sensor Fault Diagnosis Based on Sliding Mode Observer for Permanent Magnet Synchronous Traction Motor. In Proceedings of the 2018 IEEE 27th International Symposium on Industrial Electronics (ISIE), Cairns, Australia, 13–15 June 2018; pp. 835–840. [CrossRef]
22. Foo, G.H.B.; Zhang, X.; Vilathgamuwa, D.M. A Sensor Fault Detection and Isolation Method in Interior Permanent-Magnet Synchronous Motor Drives Based on an Extended Kalman Filter. *IEEE Trans. Ind. Electron.* **2013**, *60*, 3485–3495. [CrossRef]
23. Kommuri, S.K.; Lee, S.B.; Veluvolu, K.C. Robust Sensors-Fault-Tolerance with Sliding Mode Estimation and Control for PMSM Drives. *IEEE/ASME Trans. Mechatron.* **2018**, *23*, 17–28. [CrossRef]
24. Dybkowski, M.; Klimkowski, K. Stator current sensor fault detection and isolation for vector controlled induction motor drive. In Proceedings of the IEEE International Power Electronics and Motion Control Conference (PEMC), Varna, Bulgaria, 25–28 September 2016; pp. 1097–1102.
25. El Khil, S.K.; Jlassi, I.; Estima, J.O.; Mrabet-Bellaaj, N.; Cardoso, A.J.M. Detection and isolation of open-switch and current sensor faults in PMSM drives, through stator current analysis. In Proceedings of the 2017 IEEE 11th International Symposium on Diagnostics for Electrical Machines, Power Electronics and Drives (SDEMPED), Tinos, Greece, 29 August–1 September 2017; pp. 373–379. [CrossRef]
26. El Khil, S.K.; Jlassi, I.; Estima, J.; Mrabet-Bellaaj, N.; Cardoso, A.M. Current sensor fault detection and isolation method for PMSM drives, using average normalised currents. *Electron. Lett.* **2016**, *52*, 1434–1436. [CrossRef]
27. Li, H.; Qian, Y.; Asgarpoor, S.; Sharif, H. Machine Current Sensor FDI Strategy in PMSMs. *IEEE Access* **2019**, *7*, 158575–158583. [CrossRef]
28. Li, H.; Qian, Y.; Asgarpoor, S.; Sharif, H. PMSM Current Sensor FDI Based on DC Link Current Estimation. In Proceedings of the 2018 IEEE 88th Vehicular Technology Conference (VTC-Fall), Chicago, IL, USA, 27–30 August 2018; pp. 1–5. [CrossRef]
29. Jlassi, I.; Cardoso, A.J.M. A single fault diagnostics approach for power switches, speed sensors and current sensors in regenerative PMSM drives. In Proceedings of the 2017 IEEE 11th International Symposium on Diagnostics for Electrical Machines, Power Electronics and Drives (SDEMPED), Tinos, Greece, 29 August–1 September 2017; pp. 366–372. [CrossRef]
30. Jankowska, K.; Dybkowski, M. A Current Sensor Fault Tolerant Control Strategy for PMSM Drive Systems Based on Cri Markers. *Energies* **2021**, *14*, 3443. [CrossRef]